crystals

MDPI

Article

Synthesis and Characterization of Perovskite-Type $[K_{1-x}Na_x]MgF_3$ Mixed Phases via the Fluorolytic Sol-Gel Synthesis

Florian Schütz, Linda Lange, Kerstin Scheurell, Gudrun Scholz and Erhard Kemnitz *

Department of Chemistry, Humboldt-Universität zu Berlin, 12489 Berlin, Germany; schuetzf@hu-berlin.de (F.S.); lindalange92@emailn.de (L.L.); scheurek@rz.hu-berlin.de (K.S.); gudrun.scholz@chemie.hu-berlin.de (G.S.)

* Correspondence: erhard.kemnitz@chemie.hu-berlin.de; Tel.: +49-30-2093-7555

Received: 18 January 2018; Accepted: 27 January 2018; Published: 30 January 2018

Abstract: The focus of this article is the synthesis of perovskite-type $[K_{1-x}Na_x]MgF_3$ mixed phases via the room-temperature fluorolytic sol-gel approach. Different molar ratios of K/Na were examined and analyzed by ^{19}F MAS NMR and X-ray powder diffraction. Starting from pure $KMgF_3$, a systematic substitution of potassium by sodium was evidenced when replacing K by Na. As long as the amount of sodium is less than 80% as compared to potassium, spectra just show $[K_{4-x}Na_xF]$ environments in a $[K_{1-x}Na_x]MgF_3$ mixed phase but separate structures appear when the amount of sodium is further increased. Moreover, colloidal dispersions of nanoscaled $KMgF_3$ particles were obtained, which were used to fabricate coatings on glass slides. Thin films showed antireflective behavior and high transmittance.

Keywords: nano; fluorperowskite; fluorolytic sol-gel synthesis; K for Na replacement

1. Introduction

In 2003, our group explored the fluorolytic sol-gel synthesis [1]. In contrast to the common aqueous sol-gel synthesis which leads to the formation of nanosized metal oxides, the fluorolytic sol-gel synthesis yields metal fluoride nanoparticles [2,3]. Because of the low refractive indexes of metal fluorides, obtained metal fluoride sols can be used to fabricate antireflective thin films on different substrates, e.g., glasses or polymers, *via* dip coating. Additionally, these sols can be subsequently processed to xerogels as well. This is achieved by evaporating the solvent and yields solid metal fluorides with high surface areas. Diversification of the general fluorolytic synthesis approach resulted in the access of a wide variety of fluoride based materials [4,5]. In addition, in this case, the powerful room temperature synthesis method is used to access homodispersed perovskite-type mixed phases of $[K_{1-x}Na_x]MgF_3$ on a nano-scaled dimension under ambient conditions. For many decades, scientists are dealing with perovskite-type compounds like $KMgF_3$ and $NaMgF_3$ for different purposes, especially because of their interesting physical properties [6,7], synthetic accessibility [8,9], and application-focused demands [10,11]. Furthermore, the synthesis of mixed phases was investigated and will be used for direct comparison [12]. In general, compounds like $KMgF_3$ act as high-performance ceramics and luminescence host matrices [13–15]. Hence, the synthetic access of nanosized $[K_{1-x}Na_x]MgF_3$ mixed phases via the fluorolytic sol-gel synthesis under ambient conditions, their characterization, and probing their applicability for antireflective coatings is the main focus of this article.

2. Methods and Experimental

2.1. Methods

^{19}F MAS NMR: ^{19}F MAS NMR data were measured with a Bruker Advance 400 MHz spectrometer (Billerica, MA, USA). All dried powder samples were filled into 2.5 mm ZrO_2 rotors and the main rotation frequency was applied at 20 kHz. Referred to $\delta = 0$ ppm of $CFCl_3$ (using α-AlF_3 as the secondary standard for calibration) and with a D_1 time of 5 s, every spectrum consists of 32 scans.

XRD: Powder diffraction analysis was done by a Seifert XRD 3003 TT (Schnaittach-Hormersdorf, Germany) with rotating sample holder using Cu radiation (Cu $K_{\alpha 1,2}$; $\lambda = 1.54$ Å; U = 40 kV; I = 40 mA; Ni filter). All samples were measured in Bragg-Bretano geometry and results compared to powder diffraction files of COD-inorganic.

Dip-Coating: To fabricate thin films from nanoscopic dispersions, float glasses (40 mm × 20 mm × 3 mm) were coated by dip coating. To ensure a layer thickness of d > 100 nm, the dip-coating process was repeated three times. Obtained layers were heated up to 450 °C with a heating rate (HR) of 10 K·min^{-1}, and kept at this temperature for 15 min.

Transmission-Spectroscopy: Layer thickness (d), reflectance (R_{min}), transmission (T_{max}), and refractive index n, using a FILMetrics Thin Film Analyzer F10-RT (Unterhaching, Germany) were determined. Spectra were measured in a wavelength range of λ = 400–1050 nm.

2.2. Experimental

Materials:

Compound	Formula	Concentration/Purity	Supplier
Magnesium Ethoxide	$Mg(OEt)_2$	99.8%	EVONIK Industries
Magnesium Chloride	$MgCl_2$	anhydrous, ≥98%	Aldrich
Potassium Methoxide	KOMe	≥95%	Aldrich
Hydrogen Fluoride	HF	anhydrous, pure	Solvay
Methanol	MeOH	≥99.6%	Aldrich
HF solution in Methanol	HF_{MeOH}	20.53 mol·L^{-1}	-

Synthesis of HF_{MEOH}: The alcoholic HF solution was prepared according to our previous report by dissolving HF in methanol [4].

Synthesis of $KMgF_3$ (coating sol): 100 mL MeOH, 2.99 mL HF_{MeOH} (60 mmol), and 0.1 mL nitric acid (2 mmol) were added in a 250 mL PP bottle. In a schlenk flask, 1.40 g KOMe (20 mmol) and 2.29 g $Mg(OEt)_2$ (20 mmol) were dissolved in 90 mL MeOH. The grey solution of the potassium and magnesium precursors were transferred dropwise into the HF/HNO_3 solution under heavy stirring. After one day, the grey dispersion turned into a milky sol and 0.3 mL TMOS (2 mmol) were added. After 7 days of stirring, a clear, colorless sol was obtained.

Synthesis of $NaMgF_3$: 100 mL MeOH, 2.99 mL HF_{MeOH} (60 mmol), and 0.1 mL nitric acid (2 mmol) were added in a 250 mL PP bottle. In a schlenk flask, 0.46 g Na (20 mmol) and 2.29 g $Mg(OEt)_2$ (20 mmol) were dissolved in 90 mL MeOH. The grey solution of the sodium and magnesium precursors were transferred dropwise into the HF/HNO_3 solution under heavy stirring. After one day, an additive (Table 1) was added. After 7 days of stirring, a grey opaque dispersion was obtained.

Xerogel: 40 mL of $NaMgF_3$ sol were put into a glass flask. The solvent was removed under vacuum and the obtained powder was divided into three parts, whereas two were thermally treated at different temperatures.

Synthesis of $[K_{1-x}Na_x]MgF_3$: 100 mL MeOH, 2.99 mL HF_{MeOH} (60 mmol), and 0.1 mL nitric acid (2 mmol) were added in a 250 mL PP bottle. In a schlenk flask, Na (Table 2), KOMe (Table 2) and 2.29 g $Mg(OEt)_2$ (20 mmol) were dissolved in 90 mL MeOH. The grey solution of the sodium/potassium and magnesium precursors were transferred dropwise into the HF/HNO_3 solution under heavy stirring.

After one day, an additive (Table 1) was added. After 7 days of stirring, a grey opaque dispersion was obtained.

Xerogel: 40 mL of $[K_{1-x}Na_x]MgF_3$ sol were put into a glass flask. The solvent was removed under vacuum and the obtained powder was divided into three parts, whereas two were thermally treated at different temperatures.

Table 1. Amounts of Additives in $[K_{(1-x)}Na_x]MgF_3$ syntheses.

Additive	$n_{Additive}$ [mmol]	$v_{Additive}$ [mL]
TFA	2	0.15
$Al(O^sBu)_3$	2	0.50
$Zr(O^iPr)_4$	2	0.62
TMOS	2	0.30

TFA: Trifluoro acetic acid, TMOS: Tetramethoxysilane. *s: sec-*, *i: iso-*.

Table 2. Amounts of reactants in $[K_{(1-x)}Na_x]MgF_3$ syntheses.

Compound	n_{Na} [mmol]	m_{Na} [g]	n_{KOMe} [mmol]	m_{KOMe} [g]
$[K_{0.2}Na_{0.8}]F_3$	16	0.37	4	0.28
$[K_{0.4}Na_{0.6}]F_3$	12	0.28	8	0.56
$[K_{0.6}Na_{0.4}]F_3$	8	0.18	12	0.84
$[K_{0.8}Na_{0.2}]F_3$	4	0.09	16	1.12

3. Results and Discussion

$[K_{1-x}Na_x]MgF_3$ phases of varying K to Na ratios were synthesized according the following general reaction stoichiometry (Scheme 1).

$$(1-x)\ \mathrm{KOMe} + x\ \mathrm{Na} + \mathrm{Mg(OEt)_2} + 3\ \mathrm{HF_{MeOH}} \rightarrow [K_{1-x}Na_x]MgF_3 + 2\ \mathrm{EtOH} + \mathrm{MeOH} + x\ \mathrm{H_2}$$

whereas: $x = 1, 0.8, 0.6, 0.4, 0.2, 0$

Scheme 1. Formation of $[K_{1-x}Na_x]MgF_3$ by fluorolytic sol-gel synthesis.

In addition to the reaction presented in the scheme above, $Mg(OEt)_2$ was partly replaced by $MgCl_2$ (10–30%). In analogy to our previous report, the idea was to generate a catalytic cycle in which HCl, formed by the reaction of $MgCl_2$ with HF, would increase the reaction rate significantly due to the higher acidity of HCl as comapred to HF [4]. Unfortunately, the usage of $MgCl_2$ within this reaction leads to the formation of [K/Na]Cl, and hence, is not recommended for this reaction system. Thus, we tried to create a new catalytic cycle based on nitric acid: comparing the acidity of nitric acid sand hydrogen fluoride, nitric acid is a better proton donator towards metal–oxygen bonds than HF. Fortunately, metal nitrates react subsequently with HF forming $[K_{1-x}Na_x]MgF_3$ mixed phases without any side products.

With the focus on easily access clear sols, which indicates the formation of mainly homodispersed nanoparticles inside the sol, we investigated the influence of temperature on clearing up rate during $KMgF_3$ syntheses (Table 3). Thus, it turns out that clear sols can only be obtained by performing the synthesis under cooling. To ensure a long-time stability of the obtained sols, different additives were tested in order to avoid particle agglomeration and water induced gelation. Moreover, the addition of zeta-potential affecting electrolytes allows a faster clearing up of the $KMgF_3$-sols. Especially tetramethoxysilane (TMOS) and trifluoroacetic acid (TFA) turned out to cause a fast clearing up of the reaction systems resulting in very fast formation of clear sols. Comparing the visual appearance of different samples, the influence of TMOS and TFA is conspicuous (Figure 1). Based on dynamic light scattering (DLS) investigations, a mean particle size diameter of d = 69 nm within sol **12** was determined

(Figure 2). It can be seen that the majority of the particles exhibit diameters less than 50 nm. Moreover, the correlation curve appears to be sigmoidal, which basically indicates a monodispers contribution.

Table 3. Parameters of $KMgF_3$ syntheses.

#	Concentration [mol/L]	Temperature [°C]	Additive	Appearance
1	0.2	23	TFA	opaque
2			$Al(O^sBu)_3$	opaque
3			$Zr(O^iPr)_4$	opaque
4			TMOS	slightly opaque
5		40	TFA	opaque
6			$Al(O^sBu)_3$	opaque
7			$Zr(O^iPr)_4$	opaque
8			TMOS	opaque
9		0	TFA	slightly milky
10			$Al(O^sBu)_3$	opaque
11			$Zr(O^iPr)_4$	opaque
12			TMOS	clear

TFA: Trifluoroacetic acid, TMOS: Tetramethoxysilane. *s: sec-*, *i: iso-*.

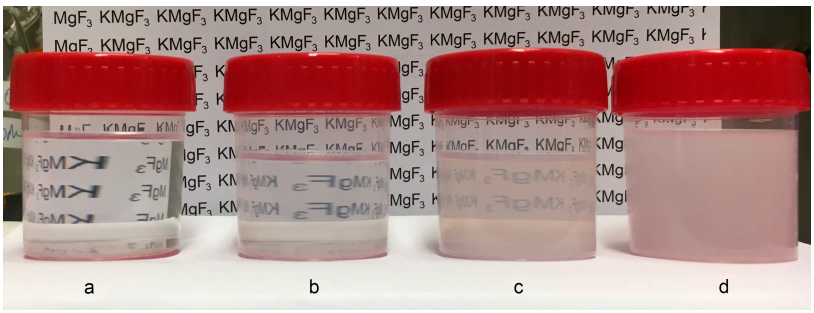

Figure 1. Comparison of visual appearances. (**a**) ethanol, (**b**) sol **12**, (**c**) sol **9**, (**d**) sol **10**.

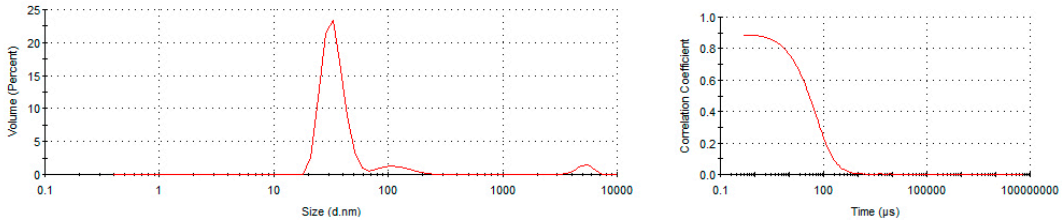

Figure 2. Volume weighted particle size distribution (**Left**) and corresponding correlation curve (**Right**) of sol **12**.

To understand the action of the sol-stabilizing additives TMOS and TFA more precisely, IR-measurements of xerogel **9** and **12** (obtained from sol **9** and **12**) were performed (Figure 3). Comparing the IR spectra of obtained xerogels to pure additives, it can be seen that xerogel **9** shows similar stretching bands to pure TFA. Especially the shifting of the C=O band from1760 cm^{-1} (purple) to 1685 cm^{-1} (orange) supports the supposition of a coordinative bonding between the Lewis acidic sites of the nanoparticle and the trifluoro acetic acid molecules. Thus, electrons of the C=O HOMO drain off, leading to a weaker bonding and a red-shifted band within the IR spectrum. In contrast to this, no traces of TMOS within xerogel **12** were found, which may be taken as an indication for the zeta-potential affecting properties of TMOS.

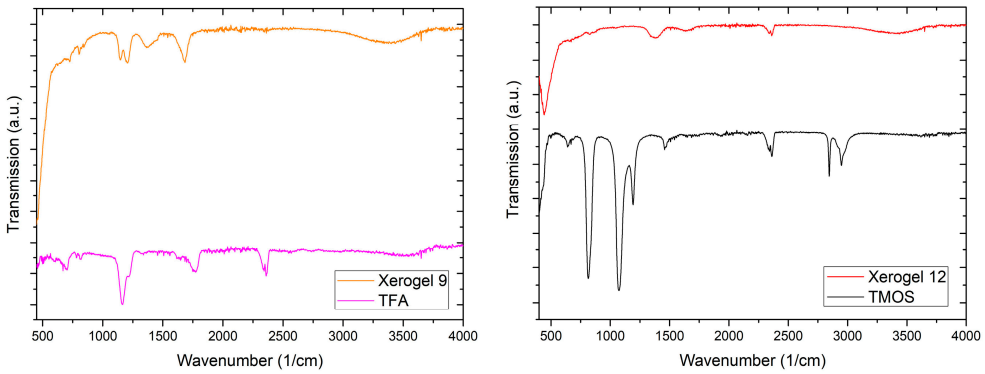

Figure 3. IR spectra of xerogel **9** (orange) and TFA (purple) (**Left**), IR spectra of xerogel 12 and TMOS (black) (**Right**).

To receive structural information, obtained X-ray amorphous xerogel **12** was thermally treated at 450 °C to increase crystallinity and to allow analysis by XRD. The ^{19}F MAS NMR spectra of non-annealed sample of xerogel **12** show the main signal of $KMgF_3$ at −184.6 ppm (Figure 4) [12]. Moreover, a small signal for MgF_2 can be found at −198.2 ppm [4]. Thermally induced changes in the structure were not confirmed by comparing ^{19}F MAS NMR spectra, but by XRD. While the non-annealed perovskite-type mixed phases of $[K_{1-x}Na_x]MgF_3$. xerogel is totally amorphous, the annealed xerogel shows good agreement with the powder diffraction file of $KMgF_3$ (Figure 5, pdf: 18-1033, star). Hence, just amorphous $KMgF_3$ can evidently be obtained not only via hydrothermal synthesis as described in literature but also via the fluorolytic sol-gel synthesis very easily under ambient conditions [9].

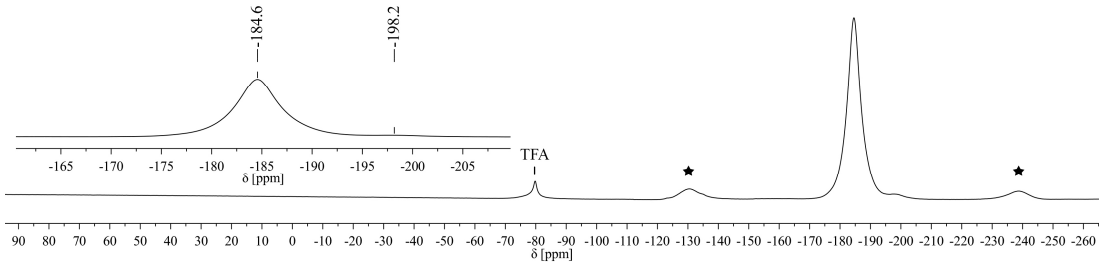

Figure 4. ^{19}F MAS NMR of non-annealed xerogel **12**, star: rotational side band, υ_{rot} = 20 kHz.

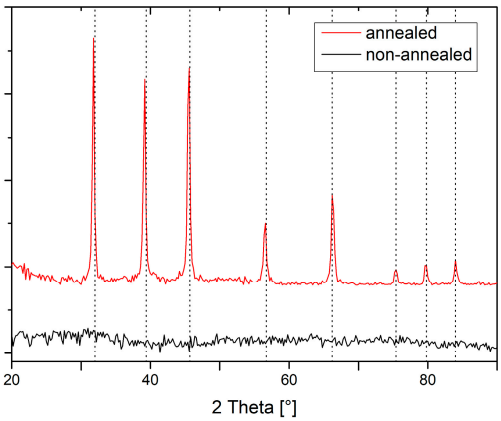

Figure 5. XRD of annealed (red) and non-annealed (black) xerogel **12**, dashed lines: $KMgF_3$ (pdf: 18-1033, star).

Based on the results described above, we tried to obtain pure $NaMgF_3$ and $[K_{1-x}Na_x]MgF_3$ mixed phases the same way by cooling down the reaction mixtures and adding TMOS subsequently. Unfortunately, all sols obtained this way were not fully clear but opaque (Table 4).

Table 4. Parameters of $NaMgF_3$ and $[K_{(1-x)}Na_x]MgF_3$ syntheses.

#	Compound	Concentration [mol/L]	Temperature [°C]	Additive	Appearance
13	$NaMgF_3$	0.2	0	TMOS	Opaque
14	$[K_{0.2}Na_{0.8}]F_3$				Opaque
15	$[K_{0.4}Na_{0.6}]F_3$				Opaque
16	$[K_{0.6}Na_{0.4}]F_3$				Opaque
17	$[K_{0.8}Na_{0.2}]F_3$				Opaque

TMOS: Tetramethoxysilane.

To receive structural information of obtained $[K_{(1-x)}Na_x]MgF_3$ mixed solid phases, ^{19}F MAS NMR of annealed xerogels **9, 13–17** were compared (Figure 6). In line with literature reports, the replacement of K-cations by Na-cations can be confirmed [12]. Up to an amount of 20% of Na-doping, the cation mixed perovskite phases remain in a $KMgF_3$ structural environment; the formation of a separate $NaMgF_3$ phase can be excluded. As already mentioned before, ^{19}F MAS NMR of xerogel **9** shows the main signal of $KMgF_3$ at −184.6 ppm. With increasing Na^+ doping concentration, the spectra show a high field shifted widening. At a Na^+ doping level of 40% (xerogel **16**) a signal at −202.9 ppm appears, pointing out the formation of $[Na_4F]$ moieties. While this signal increases with higher amounts of Na^+ within the samples (xerogel **15** and **14**), the corresponding $KMgF_3$ signal decreases until complete disappearance (xerogel **13**). With the help of the dmfit program, separate signals in the range of −180 ppm and −200 ppm can be determined and allow the assignment of different fluoride ion environments within a cubic $KMgF_3$ structure (Figure 7) [16]. The dmfit simulation shows four almost equidistant ($\Delta\delta_{ave}$ = 4.3 ppm) signals with different intensities at invariable peak-widths (Table 5). The equidistant shifts to a higher field can be explained by a step-by-step substitution of K^+ by Na^+. Although it can be assumed that a statistic substitution occurs, the experimentally determined proportion for end-member environments $[K_4F]$ and $[Na_4F]$ is favored, and therefore, results given in the literature can be confirmed.

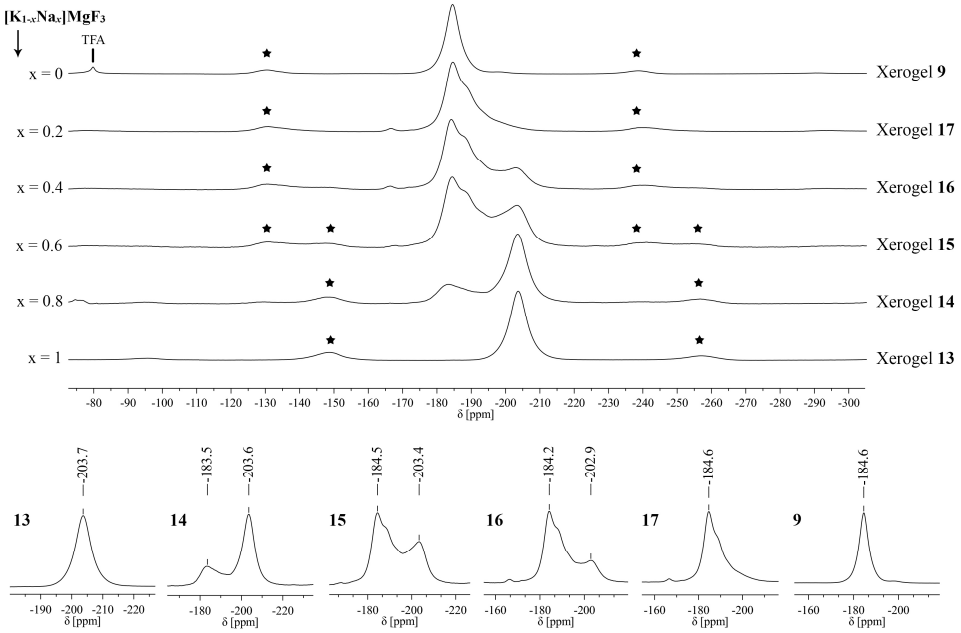

Figure 6. ^{19}F MAS NMR of xerogels **9**, **13–17**, star: spinning side band, υ_{rot} = 20 kHz.

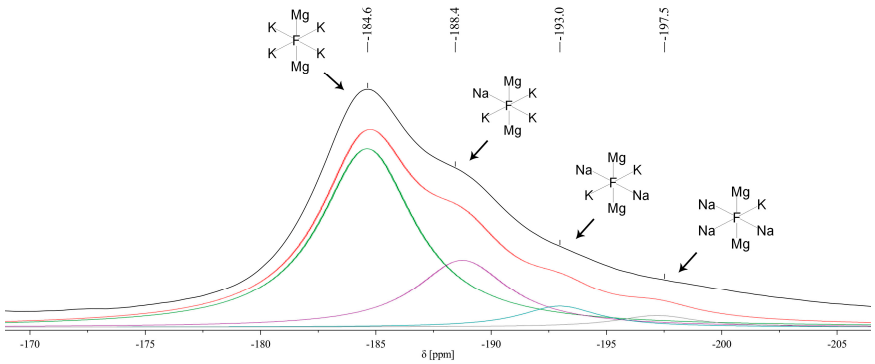

Figure 7. ^{19}F MAS NMR of xerogel **17**, dmfit analysis and corresponding fluorine sites [16].

Table 5. ^{19}F MAS NMR signals of xerogel **17** by dmfit simulation [16].

n(Na$^+$)	δ (^{19}F)$_{exp.}$ [ppm]	Δδ$_{exp.}$ [ppm]	Proportion$_{exp.}$ [%]	Proportion$_{calc.}$ [%]	n$_{exp}$(K$^+$)	n$_{calc.}$ (K$^+$)
0	−184.6	3.8 (0,1)	64.8	41.0	2.59	1.64
1	−188.4	4.6 (1,2)	24.4	41.0	0.73	1.23
2	−193.0	4.5 (2,3)	7.2	15.4	0.14	0.31
3	−197.5	-	3.6	2.6	0.04	0.03
4	-	-	0	0.2	0	0
				n$_{total}$(K$^+$)	3.50	3.21
				n$_{total}$(K$^+$)/4	0.88	0.80

This cation-replacement can also be evidenced by XRD measurements complying with the law of Vegard (Figure 8) [17]. With increasing amounts of the smaller Na-cations (r_{Na}^+ = 153 pm, r_{K}^+ = 178 pm) [18], the cell volume decreases leading to right-side shifting of peaks in the diffractograms. In comparison to the ^{19}F MAS NMR spectra, a pure $NaMgF_3$ phase cannot be found at x = 0.4. This may confirm the formation of [Na_4F] moieties within a [$K_{(1-x)}Na_x$]MgF_3 solid solution, but does not indicate the formation of pure a $NaMgF_3$ phase. The varying numbers for calculated and experimentally determined n$_{total}$(K$^+$) are in line with this assumption (Table 5). Even at Na-doping level of 60%, reflections of a $NaMgF_3$ phase are difficult to identify, whereas reflections of both compounds show up at Na-levels ≥80% [$K_{0.2}Na_{0.8}$]MgF_3.

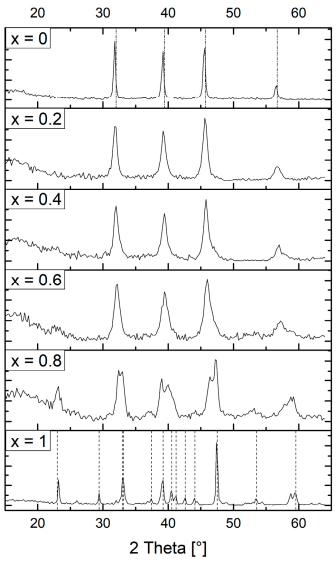

Figure 8. XRDs of annealed xerogels **9**, **13**–**17**, pdf$_{x=0}$: 18-1033, star, pdf$_{x=1}$: 81-952.

Concerning the fact that sol **12** represents a water clear colorless sol, it was used for dip coating on glass-slides. After dip coating, glass slides were thermally treated at 450 °C for 15 min. The obtained thin films show nearly perfect antireflective behavior with a remaining reflectance of just R = 0.15% and transmission as high as T = 96.1% (Figure 9, Table 6).

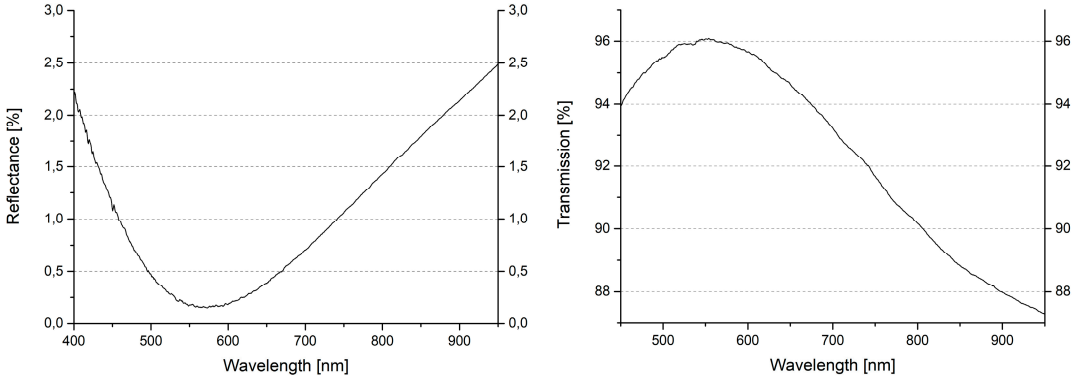

Figure 9. Reflectance and transmission curves of $KMgF_3$ thin film.

Table 6. Overview of layer properties.

Layer	T [°C]	t [min]	dT [°C/min]	d [nm]	R [%]	T [%]	$n_{632,8nm}$
1	450	15	10	116.7	0.15	96.1	1.27

4. Summary

Employing the room-temperature fluorolytic sol-gel synthesis, the formation of $KMgF_3$, $NaMgF_3$, and $[K_{1-x}Na_x]MgF_3$ mixed phases was evidenced. However, only with pure $KMgF_3$ colorless and water clear sols were they obtained when the synthesis was performed under ice bath cooling and with the addition of TMOS as a stabilizer. With the help of ^{19}F MAS NMR and XRD, we obtained evidence for the consecutive occupancy of potassium by sodium sites within a cubic $KMgF_3$ structure. If the Na dopant concentration exceeds 20% in relation to K, the formation of $[Na_4F]$ environments takes place and can be observed in ^{19}F MAS NMR. In addition, the substitution does not take place statistically, instead, end-membered environments are favored. The appearance of a pure $NaMgF_3$ phase within samples with less than 80% Na^+ can be denied as evidenced by XRD measurements. Thin films, which were obtained by dip coating with clear $KMgF_3$ sols showed very low remaining reflectance and high transmission.

Acknowledgments: The authors thank the research training network GRK 1582/2 "Fluorine as a Key Element" of DFG (Deutsche Forschungsgemeinschaft) for funding. This project was partly also funded by the German Federal Ministry of Economics and Technology (Grant 03ET1235C).

Author Contributions: Florian Schütz wrote the paper and did the experiments with the help of Linda Lange. Kerstin Scheurell and Gudrun Scholz analyzed, evaluated and discussed the NMR data. Erhard Kemnitz was responsible for coordinating the experiments and correcting the manuscript.

Conflicts of Interest: The authors declare no conflict of interest.

References

1. Kemnitz, E.; Groß, U.; Rüdiger, S.; Shekar, C.S. Amorphe metallfluoride mit außergewöhnlich großer spezifischer oberfläche. *Angew. Chem.* **2003**, *115*, 4383–4386. [CrossRef]
2. Hench, L.L.; West, J.K. The sol-gel process. *Chem. Rev.* **1990**, *90*, 33–72. [CrossRef]
3. Rudiger, S.; Kemnitz, E. The fluorolytic sol-gel route to metal fluorides-a versatile process opening a variety of application fields. *Dalton Trans.* **2008**, 1117–1127. [CrossRef] [PubMed]

4. Krahl, T.; Broßke, D.; Scheurell, K.; Lintner, B.; Kemnitz, E. Novel aspects in the chemistry of the non-aqueous fluorolytic sol–gel synthesis of nanoscaled homodisperse MgF_2 sols for antireflective coatings. *J. Mater. Chem. C Mater. Opt. Electron. Devices* **2016**, *4*, 1454–1466. [CrossRef]
5. Rehmer, A.; Scheurell, K.; Kemnitz, E. Formation of nanoscopic CaF_2 via a fluorolytic sol-gel process for antireflective coatings. *J. Mater. Chem. C Mater. Opt. Electron. Devices* **2015**, *3*, 1716–1723. [CrossRef]
6. Adamkovičová, K.; Fellner, P.; Kosa, L.; Nerad, I.; Proks, I.; Strečko, J. Determination of the enthalpy of fusion of $NaMgF_3$ and $KMgF_3$. *Thermochim. Acta* **1994**, *242*, 23–26. [CrossRef]
7. Sahnoun, M.; Zbiri, M.; Daul, C.; Khenata, R.; Baltache, H.; Driz, M. Full potential calculation of structural, electronic and optical properties of $KMgF_3$. *Mater. Chem. Phys.* **2005**, *91*, 185–191. [CrossRef]
8. Sevonkaev, I.; Goia, D.V.; Matijević, E. Formation and structure of cubic particles of sodium magnesium fluoride (neighborite). *J. Colloid Interface Sci.* **2008**, *317*, 130–136. [CrossRef] [PubMed]
9. Zhao, C.; Feng, S.; Chao, Z.; Shi, C.; Xu, R.; Ni, J. Hydrothermal synthesis of the complex fluorides $LiBaF_3$ and $KMgF_3$ with perovskite structures under mild conditions. *Chem. Commun.* **1996**, 1641–1642. [CrossRef]
10. Dotzler, C.; Williams, G.V.M.; Rieser, U.; Edgar, A. Optically stimulated luminescence in $NaMgF_3$:Eu^{2+}. *Appl. Phys. Lett.* **2007**, *91*, 121910. [CrossRef]
11. Wu, M.; Song, E.H.; Chen, Z.T.; Ding, S.; Ye, S.; Zhou, J.J.; Xu, S.Q.; Zhang, Q.Y. Single-band red upconversion luminescence of Yb^{3+}–Er^{3+} via nonequivalent substitution in perovskite $KMgF_3$ nanocrystals. *J. Mater. Chem. C Mater. Opt. Electron. Devices* **2016**, *4*, 1675–1684. [CrossRef]
12. Martin, C.D.; Chaudhur, S.; Grey, C.P.; Parise, J.B. Effect of a-site cation radius on ordering of bx6 octahedra in (K, Na) MgF_3 perovskite. *Am. Mineral.* **2005**, *90*, 1522–1533. [CrossRef]
13. Bacci, C.; Fioravanti, S.; Furetta, C.; Missouri, M.; Ramogida, G.; Rossetti, R.; Sanipoli, C.; Scacco, A. Photoluminescence and thermally stimulated luminescence in $KMgF_3$:Eu^{2+} crystals. *Radiat. Prot. Dosim.* **1993**, *47*, 277–280. [CrossRef]
14. Bhalla, A.S.; Guo, R.; Roy, R. The perovskite structure—A review of its role in ceramic science and technology. *Mater. Res. Innov.* **2000**, *4*, 3–26. [CrossRef]
15. Furetta, C.; Bacci, C.; Rispoli, B.; Sanipoli, C.; Scacco, A. Luminescence and dosimetric performances of $KMgF_3$ crystals doped with metal impurity ions. *Radiat. Prot. Dosim.* **1990**, *33*, 107–110. [CrossRef]
16. Massiot, D.; Fayon, F.; Capron, M.; King, I.; Le Calvé, S.; Alonso, B.; Durand, J.-O.; Bujoli, B.; Gan, Z.; Hoatson, G. Modelling one- and two-dimensional solid-state NMR spectra. *Magn. Reson. Chem.* **2002**, *40*, 70–76. [CrossRef]
17. Vegard, L. Die konstitution der mischkristalle und die raumfüllung der atome. *Z. Phys.* **1921**, *5*, 17–26. [CrossRef]
18. Shannon, R.T.; Prewitt, C.T. Effective ionic radii in oxides and fluorides. *Acta Crystallogr. B Struct. Crystallogr. Crys. Chem.* **1969**, *25*, 925–946. [CrossRef]